Analytical approach to modulation properties of quantum dot lasers

Cite as: J. Appl. Phys. **109**, 103112 (2011); https://doi.org/10.1063/1.3587244
Submitted: 04 April 2011 • Accepted: 06 April 2011 • Published Online: 20 May 2011

Kathy Lüdge, Eckehard Schöll, Evgeny Viktorov, et al.

Analytical approach to modulation properties of quantum dot lasers

Kathy Lüdge,[1,a)] Eckehard Schöll,[1] Evgeny Viktorov,[2] and Thomas Erneux[2]
[1]*Institut für Theoretische Physik, Technische Universität Berlin, Hardenbergstr. 36, 10623 Berlin, Germany*
[2]*Université Libre de Bruxelles, Optique Nonlinéaire Théorique, Campus Plaine, C.P. 231, 1050 Bruxelles, Belgium*

(Received 4 April 2011; accepted 6 April 2011; published online 20 May 2011)

We analyze a microscopically based rate equation model for quantum dot lasers. The model separately treats the dynamics of electrons and holes, and the carrier-carrier scattering rates depend nonlinearly on the wetting layer carrier densities. Our objective is to determine analytical expressions for the relaxation oscillation frequency and damping rate. To this end, we consider the Class B limit of the five rate equations and apply asymptotic techniques. We consider two cases corresponding to either equivalent or drastically different decay rates for the electrons and holes. We show how they contribute to increase the relaxation oscillation damping rate compared to the damping rate of the conventional laser and that there exist optimal conditions on the control parameters in order to observe maximum damping. © *2011 American Institute of Physics*.
[doi:10.1063/1.3587244]

I. INTRODUCTION

A quantum dot (QD) laser is a semiconductor laser (SL) that uses quantum dots as the active laser medium in its light-emitting region. Due to the tight confinement of charge carriers in QDs, they exhibit an electronic structure similar to atoms. Lasers fabricated from such an active medium exhibit higher device performances compared to traditional semiconductor lasers based on bulk or quantum well active medium. Improvements in modulation bandwidth, lasing threshold, relative intensity noise, linewidth enhancement factor, and temperature insensitivity have all been reported.[1,2] Although QD lasers have raised an enormous interest in the physical community, their modeling in terms of rate equations remains a delicate task. In contrast to quantum well lasers, for which two rate equations are successfully used to describe a variety of setups,[3–7] the dynamical response of current QD lasers seem to strongly depend on the way they are fabricated and on the operating wavelength. Both excitonic and electron-hole models have been developed to describe turn-on experiments,[8,9] gain recovery dynamics,[10–14] optical injection,[15,16] and optical feedback.[17–19]

Excitonic rate equation models assume the same scattering rates for electrons and holes. They allow the derivation of simple analytical expressions, which are useful when examining experimental data. However, they are not capable of connecting the QD structure and its material composition with the device performance. Electron-hole rate equation models take into account that the thermal redistribution occurs on different time scales for holes and electrons. These models aim to bridge the gap between a full microscopic description and the simple excitonic models.

The electron-hole rate equation model that we consider here involves five independent variables for the charge carrier densities in the QD; the carrier densities in the carrier reservoir, which is given by a quantum well structure or wetting layer (WL); and the photon density. The model was introduced in Ref. 20, and studied in detail since then in Refs. 8 and 9. The scattering rates are calculated microscopically within the Boltzmann equation and orthogonalized plane wave approach. The computed scattering rates are found to be strongly nonlinear functions of the WL carrier densities, and all dynamical experiments (turn-on, modulation response, optical feedback) need to be simulated numerically.

Our laser problem depends on several parameters that admit large ranges of values. Moreover, the solution of the laser equations exhibits different time scales, which require accurate simulations. In this paper, we show that there exists an alternative to computationally expensive studies by using analytical approximations. Because our analysis is not a routine application of asymptotic techniques, we explain each step in detail. We obtain analytical expressions for the relaxation properties of the laser and show how a deeper understanding of the effect of key parameters can be found. We evaluate the validity of all our results by comparing analytical and numerical data.

In order to simplify our five rate equations, we recall that semiconductor lasers are class B lasers and apply approximation techniques appropriate for this class of lasers.[21] Class B lasers include most practical lasers used in applications and in laboratories (semiconductor lasers, CO_2 lasers, and solid state lasers). When a Class B laser is disturbed during operation, e.g., by fluctuations of the pump power, its output power does not immediately return to its steady state. This slow decay results from the fact that the upper-state material lifetime is longer than the cavity lifetime. Changes in pump power typically lead to damped relaxation oscillations (RO). Because of the different lifetimes of the carriers and the photons in the cavity, asymptotic techniques can be applied.[21] The main objective of this paper is to determine expressions for the RO frequency in QD lasers and for its damping rate. We consider two cases

a)Author to whom correspondence should be addressed. Electronic mail: luedge@physik.tu-berlin.de.

corresponding to either equivalent or drastically different decay rates for the electrons and holes. As we shall demonstrate, distinct asymptotic limits appear for these two cases. All our analytical expressions are compared to data obtained numerically by solving the complete laser rate equations.

The plan of the paper is as follows. Section II introduces the original laser equations and determines properties of the nonzero intensity steady state. In Sec. III, we reformulate the five laser equations in dimensionless form and apply the Class B limit. The structure of the resulting equations then shows that the dynamical problem can be reduced to three rate equations, in first approximation. We study these equations in the case of similar and different decay rates of the electrons and holes. The analysis is described in detail in Secs. III A and III B, respectively. Section IV contains our comparison between analytical and numerical data in the case of different decay rates of electrons and holes. Finally, Sec. V summarizes our main results.

II. LASER MODEL

In this paper, we consider the electron-hole rate equation model previously studied in Refs. 8 and 9. In the QD laser, the carriers are first injected into the two-dimensional carrier reservoir (WL) before being captured by the QDs. The model considers a system for electrons and holes in the QD ground state (GS) which typically applies for the self-organized QDs in the InAs/InGaAs material system. The nonlinear rate equations describe the dynamics of the charge carrier densities in the QD, n_e and n_h; the carrier densities in the WL, w_e and w_h (e and h stand for electrons and holes, respectively); and the photon density, n_{ph}. They are of the form

$$\dot{n}_e = S_e^{in} N^{QD} - \frac{1}{\tau_e} n_e - R_{ind}(n_e, n_h, n_{ph}) - R_{sp}(n_e, n_h), \quad (1)$$

$$\dot{n}_h = S_h^{in} N^{QD} - \frac{1}{\tau_h} n_h - R_{ind}(n_e, n_h, n_{ph}) - R_{sp}(n_e, n_h), \quad (2)$$

$$\dot{w}_e = \eta \frac{j}{e_0} + \frac{n_e N^{sum}}{\tau_e N^{QD}} - S_e^{in} N^{sum} - \tilde{R}_{sp}(w_e, w_h), \quad (3)$$

$$\dot{w}_h = \eta \frac{j}{e_0} + \frac{n_h N^{sum}}{\tau_h N^{QD}} - S_h^{in} N^{sum} - \tilde{R}_{sp}(w_e, w_h), \quad (4)$$

$$\dot{n}_{ph} = -2\kappa n_{ph} + \Gamma R_{ind}(n_e, n_h, n_{ph}) + \beta R_{sp}(n_e, n_h). \quad (5)$$

In these equations, the nonlinear Coulomb scattering rates are denoted by S_e^{in} and S_h^{in} for electron and hole capture into the QD levels and by S_e^{out} and S_h^{out} for carrier escape to the WL, respectively. S_e^{out} and S_h^{out} appear in the scattering times $\tau_e \equiv (S_e^{in} + S_e^{out})^{-1}$ and $\tau_h \equiv (S_h^{in} + S_h^{out})^{-1}$, and they depend on w_e and w_h. The induced processes of absorption and emission are modeled by a linear gain $R_{ind} \equiv WA(n_e + n_h - N^{QD})n_{ph}$, where N^{QD} denotes twice the QD density of the lasing subgroup (*twice* accounts for spin degeneracy), W is the Einstein coefficient, and A is the WL normalization area. The density N^{sum} is twice the total QD density, as given by experimental surface imaging. The spontaneous emission in the QD is approximated by $R_{sp} \equiv (W/N^{QD}) n_e n_h$. The WL spontaneous recombination rate is described by $\tilde{R}_{sp} \equiv B^S w_e w_h$ where B^S is the band-band recombination coefficient in the WL. β is the spontaneous emission factor. Γ is the optical confinement factor, the coefficient 2κ denotes the total cavity loss, j is the injection current density, and e_0 is the elementary charge. The factor $\eta \equiv 1 - w_e/N^{WL}$ accounts for the fact that we cannot inject any more carriers if the WL is already filled ($w_e = N^{WL}$). Details and values of the parameters are documented in Ref. 8. The band structure considered for the active medium of the QD laser is depicted in Fig. 1(a). The microscopically obtained scattering times τ_e and τ_h are shown in Fig. 1(b) in the steady state as a function of the normalized pump current j/j_{th} where j_{th} is the threshold current density. We consider two specific problems corresponding to different QD structures, namely the case of similar scattering times (case S) and the cases of drastically different scattering times (case D).

We wish to simplify Eqs. (1)–(5) by taking advantage of the natural values of the parameters. To this end, we first need to reformulate these equations in dimensionless form. Specifically, we introduce the new dimensionless variables N_{ph}, $N_{e/h}$, $W_{e/h}$, and t' defined by:

$$\begin{aligned} n_{ph} &= A^{-1} N_{ph}, \quad n_{e/h} = N^{QD} N_{e/h}, \\ w_{e/h} &= N^{sum} W_{e/h}, \quad t' \equiv 2\kappa t. \end{aligned} \quad (6)$$

Inserting (6) into Eqs. (1)–(5), and neglecting spontaneous emission in the photon equation, we obtain

$$N_e' = \gamma\left[F_e(N_e, W_e, W_h) - (N_e + N_h - 1)N_{ph} - N_e N_h\right], \quad (7)$$

$$N_h' = \gamma\left[F_h(N_h, W_e, W_h) - (N_e + N_h - 1)N_{ph} - N_e N_h\right], \quad (8)$$

$$W_e' = \gamma[\eta J - F_e(N_e, W_e, W_h) - cW_e W_h], \quad (9)$$

$$W_h' = \gamma[\eta J - F_h(N_h, W_e, W_h) - cW_e W_h], \quad (10)$$

$$N_{ph}' = N_{ph}[-1 + g(N_e + N_h - 1)] \quad (11)$$

where prime means differentiation with respect to dimensionless time t'. The dimensionless functions F_e, F_h, and η, and parameters g, c, J, and γ are defined by

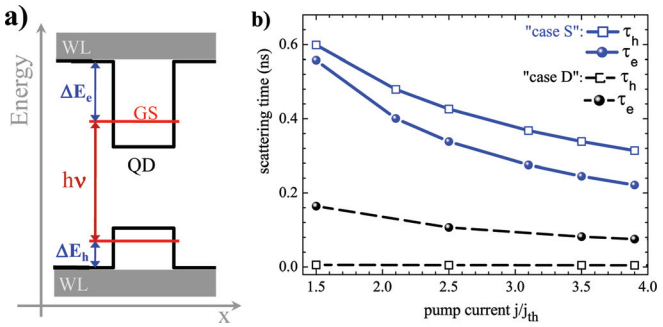

FIG. 1. (Color online) (a) Scheme of the band structure across the active medium of the QD laser. (b) Steady state electron and hole scattering times τ_e (circles) and τ_h (squares), respectively, for Coulomb scattering between WL and QD states. Blue solid and black dashed lines correspond to carrier lifetimes of different QD structures: The confinement energies between QD ground state and QW band edge are $\Delta E_e = 140$ meV, $\Delta E_h = 120$ meV for case S (blue solid), and $\Delta E_e = 210$ meV, $\Delta E_h = 50$ meV for case D (black dashed).

$$F_{e/h} \equiv -N_{e/h}(s^{in}_{e/h} + s^{out}_{e/h}) + s^{in}_{e/h}, \tag{12}$$

$$\eta \equiv 1 - \frac{N^{sum}}{N^{WL}} W_e, \quad s^{in/out}_{e/h} \equiv \frac{S^{in/out}_{e/h}}{W}, \tag{13}$$

$$g \equiv \frac{\Gamma W A N^{QD}}{2\kappa}, \quad c \equiv \frac{B^S N^{sum}}{W}, \tag{14}$$

$$J \equiv \frac{j}{e_0 N^{sum} W}, \quad \gamma \equiv \frac{W}{2\kappa}. \tag{15}$$

With the values of the original parameters specified in Ref. 8, we find $\gamma = 7 \times 10^{-3}$, $g \simeq 3.78$, $c = 0.14$, and $N^{sum}/N^{WL} = 10^{-2}$. We neglect the small correction term for η in (13) and use $\eta = 1$. Next, we investigate the asymptotic limit $\gamma \to 0$, keeping all remaining parameters fixed. This limit is singular because setting $\gamma = 0$ into the rate equations implies that all population variables are constant and that N_{ph} is either decreasing or increasing exponentially. This conclusion is physically invalid because we numerically observe decaying RO for N_{ph}. Before we describe how this singularity can be removed, it is worth stressing that simple relations can be obtained for the nonzero intensity steady state.

The carrier populations are not independent but satisfy the conservation relation $N'_e - N'_h + W'_e - W'_h = 0$, which then leads to

$$N_e - N_h + W_e - W_h = 0 \tag{16}$$

in the undoped case. The steady states satisfy Eqs. (7)–(11) with the left hand sides equal to zero. From Eq. (11) with $N'_{ph} = 0$ and $N_{ph} \neq 0$, we note that

$$N_e + N_h = \frac{1+g}{g}. \tag{17}$$

We shall use Eq. (17) several times in our stability analysis to simplify $N_e + N_h$. Together with Eq. (16), we may express N_e and N_h as functions of the WL populations

$$N_e = \frac{1}{2}\left[\frac{1+g}{g} + W_h - W_e\right], \tag{18}$$

$$N_h = \frac{1}{2}\left[\frac{1+g}{g} - W_h + W_e\right]. \tag{19}$$

Finally, using Eq. (7) and Eq. (9) with $N'_e = W'_e = 0$ and Eq. (17), we obtain an expression for N_{ph} of the form

$$N_{ph} = g(J - N_e N_h - c W_e W_h). \tag{20}$$

With N_e and N_h given by Eq. (18) and Eq. (19), respectively, we note that N_{ph} is a function of only the WL population variables. Consequently, the steady state problem is reduced to the determination of the WL population steady states, which needs to be done numerically because the scattering rates are computed numerically.

In the next section, we assume that the nonzero intensity steady state is known and investigate the time-dependent problem in terms of deviations from it. Figure 2(a) shows the numerical solution of the laser turn-on dynamics for the two cases introduced in Fig. 1(b). We note that in both cases ("case S" and "case D" shown by blue solid and black dashed lines, respectively, in Fig. 2(a)) the laser reaches its steady state via relaxation oscillations (RO). They can be strongly damped (case D) or show pronounced oscillations (case S).

III. CLASS B LIMIT

As we have previously emphasized, the limit $\gamma \to 0$ is singular, because the reduced equations if $\gamma = 0$ admit no physical solutions. We may remove the singularity by a change of variables, which has been successfully used for the conventional rate equations.[21] The key observation from

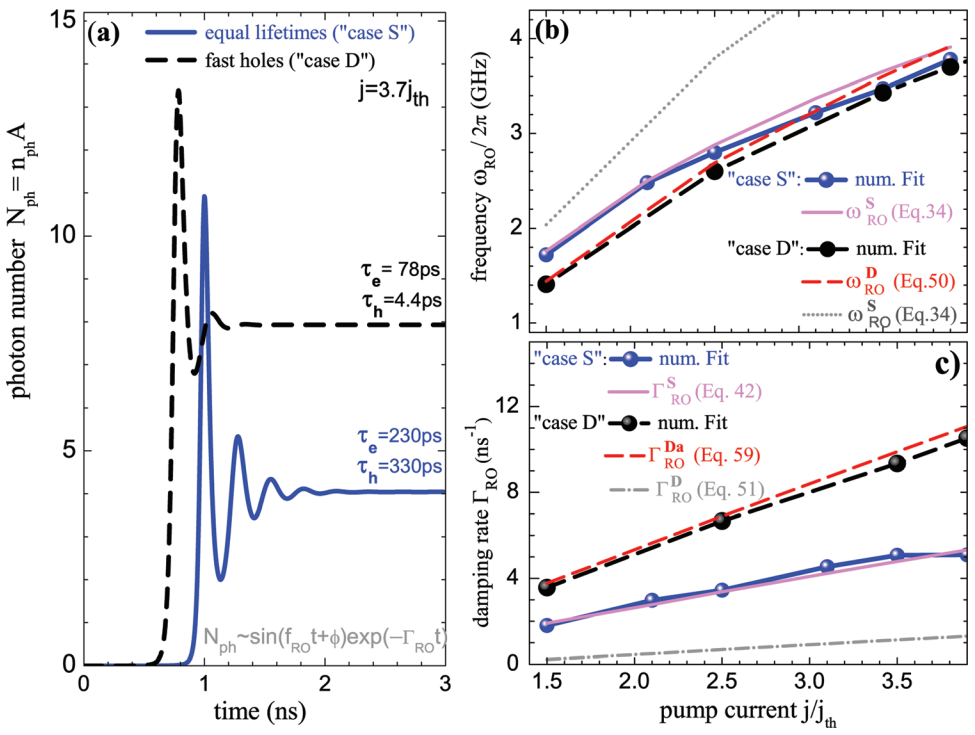

FIG. 2. (Color online) (a) Turn-on dynamics of the QD laser for case S (blue solid) and case D (black dashed) introduced in Fig. 1(b) ($j = 3.7 j_{th}$). (b), (c) Comparison between numerically fitted (symbols) and analytically obtained (lines) data for the RO frequency (b) and RO damping rate (c) The equations used for the analytic results are indicated in the legend. For the fitting, we use the expression $N_{ph} \simeq C \sin(\omega_{RO} t + \varphi) \exp(-\Gamma_{RO} t)$ to extract the linear RO frequency and damping rate from the numerical simulations.

the linear stability analysis that suggests this change of variable is the fact that the RO frequency is proportional to $\sqrt{\gamma}$ as $\gamma \to 0$. This motivates a change of the basic time variable ($s = \sqrt{\gamma}t'$), which then requires that the deviations of $N_{e/h}$ from their steady state values are proportional to $\sqrt{\gamma}$ in order to balance both sides of the equation for N_{ph}.

Specifically, we introduce the new time s and the deviations from the steady state y, $u_{e/h}$, and $v_{e/h}$, defined as

$$s = \sqrt{\gamma}\omega t', \quad N_{ph} = N_{ph}^0(1+y), \tag{21}$$

$$N_{e/h} = N_{e/h}^0 + \sqrt{\gamma}\omega g^{-1} u_{e/h}, \tag{22}$$

$$W_{e/h} = W_{e/h}^0 + \gamma\omega g^{-1} v_{e/h} \tag{23}$$

where the superscript 0 denotes the steady state, and the coefficient ω has been introduced in order to simplify the leading order evolution equations. This coefficient ω will be defined later. Note that the scaling factor $\sqrt{\gamma}$ for $N_{e/h}$ is different from the factor γ for $W_{e/h}$. This difference results from the fact that only N_e and N_h appear in the equation for N_{ph}. After simplifying and reorganizing the right-hand sides in powers of $\sqrt{\gamma}$, we obtain

$$y' = (1+y)(u_e + u_h) \tag{24}$$

$$\begin{aligned}\omega^2 u_e' = &-(s_e^{in} + s_e^{out})\sqrt{\gamma}\omega u_e - N_{ph} y \\ &- \sqrt{\gamma}\omega(u_e + u_h)N_{ph} \\ &- \sqrt{\gamma}\omega(u_e N_h + N_e u_h) + O(\gamma),\end{aligned} \tag{25}$$

$$\begin{aligned}\omega^2 u_h' = &-(s_h^{in} + s_h^{out})\sqrt{\gamma}\omega u_h - N_{ph} y \\ &- \sqrt{\gamma}\omega(u_e + u_h)N_{ph} \\ &- \sqrt{\gamma}\omega(u_e N_h + N_e u_h) + O(\gamma),\end{aligned} \tag{26}$$

$$\omega v_e' = (s_e^{in} + s_e^{out})u_e + O(\sqrt{\gamma}), \tag{27}$$

$$\omega v_h' = (s_h^{in} + s_h^{out})u_h + O(\sqrt{\gamma}) \tag{28}$$

where superscript prime now means differentiation with respect to time s. The small parameter γ is no longer multiplying the right-hand sides of the population equations. It appears through $\sqrt{\gamma}$ and γ in the right-hand sides of the equations. Setting $\gamma = 0$ leads to five equations which, as we shall later demonstrate, admit physical solutions.

Note that Eqs. (24)–(26) are three coupled equations for y, u_e, and u_h including $O(\sqrt{\gamma})$ corrections. The scattering rates $s_{e/h}^{in/out}$ depend upon $v_{e/h}$ only in $O(\gamma)$. On the other hand, Eqs. (27) and (28) indicate that $v_{e/h}$ (defined as the deviations from the steady state value of the WL carrier densities) passively follows $u_{e/h}$ (defined as the deviations from the steady state value of the QD carrier densities). Therefore, we only need to examine Eqs. (24)–(26).

A. Similar carrier lifetimes τ_e and τ_h (case S)

For large scattering times that ensure $s_e^{in} + s_e^{out}$ and $s_h^{in} + s_h^{out}$ to be $O(1)$ quantities compared with $\sqrt{\gamma}$, we may formulate the leading order problem by setting $\gamma = 0$ in Eqs. (24)–(26). We obtain the following three equations for y, u_e, and u_h:

$$y' = (1+y)(u_e + u_h) \tag{29}$$

$$\omega^2 u_e' = -N_{ph} y, \tag{30}$$

$$\omega^2 u_h' = -N_{ph} y. \tag{31}$$

Adding the two last equations, we obtain the following equations for y and $u_+ \equiv u_e + u_h$

$$u_+' = -y, \tag{32}$$

$$y' = (1+y)u_+ \tag{33}$$

provided ω is defined as $\omega^2 \equiv 2N_{ph}$ (ω was introduced as a free parameter in the definition of the time variable s in Eq. (21) and is now chosen such that Eqs. (29)–(31) appear in the simplest possible way). Eqs. (32) and (33) are conservative and admit a one-parameter family of periodic solutions.[21] Near its steady state $u_+ = y = 0$, the oscillations exhibit a frequency close to 1, which is defined as the RO frequency in units of time s. Using the definition of t' in Eq. (6) and then the definition of s in Eq. (21), the RO frequency in units of the original time t is given by

$$\omega_{RO}^S \equiv 2(N_{ph} W \kappa)^{1/2} \tag{34}$$

where the subscript S means case S and we have used the definition of γ given in Eq. (15). Eqs. (32) and (33) are conservative and do not describe how the RO oscillations are damped. We need to explore the equations for the first-order correction of the leading solution. However, we are first interested to find the linear RO damping rate because it is this quantity that we determine from the numerical simulations of the original laser equations. To this end, it is mathematically more convenient to investigate the linearized problem including both $O(1)$ and $O(\sqrt{\gamma})$ terms.

After linearizing Eqs. (24)–(26) at the steady state $y = u_e = u_h = 0$, we formulate the Jacobian matrix and determine the following characteristic equation for the growth rate λ,

$$\lambda^3 - \lambda^2 T_1 + \lambda T_2 - T_3 = 0 \tag{35}$$

where

$$\begin{aligned}T_1 = \sqrt{\gamma}\omega^{-1}[&-(s_e^{in} + s_e^{out}) - N_{ph} - N_h \\ &- (s_h^{in} + s_h^{out}) - N_{ph} - N_e],\end{aligned} \tag{36}$$

$$T_2 = 1 + O(\gamma), \tag{37}$$

$$T_3 = \frac{1}{2}\sqrt{\gamma}\omega^{-1}\left[-(s_h^{in} + s_h^{out}) - (s_e^{in} + s_e^{out})\right]. \tag{38}$$

We solve Eq. (35) by seeking a solution of the form

$$\lambda = \lambda_0 + \sqrt{\gamma}\omega^{-1}\lambda_1 + \ldots \tag{39}$$

After introducing (39) into Eq. (35), we equate to zero the coefficients of each power of $\sqrt{\gamma}$. We obtain a sequence of problems for λ_0, λ_1,.. After simplification, the solutions of the first two problems with $\lambda_0 \neq 0$ are

$$\lambda_0 = \pm i, \tag{40}$$

and

$$\lambda_1 = -\frac{1}{2}[2N_{ph} + 1 + g^{-1} + \frac{1}{2}(s_e^{in} + s_e^{out}) + \frac{1}{2}(s_h^{in} + s_h^{out})]. \tag{41}$$

Eq. (40) gives the leading approximation of the RO frequency in units of time s ($|Im(\lambda_0)| = 1$), or equivalently, the frequency Eq. (34) in units of time t. Eq. (41) shows that λ_1 is real. The leading approximation of the RO damping rate in units of time s is thus $\Gamma_{RO} = \sqrt{\gamma}\omega^{-1}\lambda_1$. In units of the original time t, we obtain

$$\Gamma_{RO}^S = \frac{W}{2}[2N_{ph} + 1 + g^{-1} + \frac{1}{2}(s_e^{in} + s_e^{out}) + \frac{1}{2}(s_h^{in} + s_h^{out})]. \tag{42}$$

The expression of the RO frequency is the same as the one for the conventional semiconductor laser.[21] The expression of the damping rate is, however, different. It contains the familiar $W(1 + 2N_{ph})/2$ term but there are some extra terms. The term g^{-1} comes from the fact that the spontaneous emission is modeled by a quadratic nonlinearity instead of the linear term used in the excitonic theory (for the chosen parameters it is a very small correction to the damping rate). The other terms are contributions from the Coulomb scattering rates.

If we compare Eqs. (34) and (42) with the values provided numerically, we find a quantitative agreement over a large range of increasing pump currents, as can be seen in Fig. 2(b) and 2(c) for the case S (blue circles and dashed lines). If we use the same expressions now with the parameters of case D (see next section), the agreement is poor. The RO frequency is overestimated by the analytical expression (see dotted gray line in Fig. 2(b)). Moreover, the damping rate is overestimated by a factor of 10 and is not shown in Fig. 2(c). The reason for the mismatch is that for case D the scattering lifetime of electrons $\tau_h \sim 5$ ps is very small and, thus, the quantity $\sqrt{\gamma}/(W\tau_h) \simeq 23$ must be now considered as an $O(1)$ quantity. We examine this case in detail in the next subsection.

B. Different carrier lifetimes τ_e and τ_h (case D)

In this case, τ_e and τ_h differ by 2 orders of magnitude and are close to $\tau_h \sim 5$ ps and $\tau_e \sim 100$ ps, respectively, which implies that

$$s_e^{in} + s_e^{out} = \frac{1}{W\tau_e} = 14.29, \tag{43}$$

$$s_h^{in} + s_h^{out} = \frac{1}{W\tau_h} = 285.71. \tag{44}$$

We note that $s_h^{in} + s_h^{out}$ is much larger than $s_e^{in} + s_e^{out}$. Because $\sqrt{\gamma} = 0.08$, it will be more accurate to assume that $(s_h^{in} + s_h^{out})\sqrt{\gamma}$ is an $O(1)$ quantity. From Eqs. (24)–(28), the leading order problem is obtained by setting $\gamma = 0$, and is given by

$$y' = (1 + y)(u_e + u_h), \tag{45}$$

$$u_e' = -\frac{1}{2}y, \tag{46}$$

$$u_h' = -\frac{1}{2}y - au_h, \tag{47}$$

where

$$a \equiv (s_h^{in} + s_h^{out})\sqrt{\gamma}\omega^{-1} = \sqrt{\frac{\gamma}{2N_{ph}}}(s_h^{in} + s_h^{out}) = \frac{1}{\omega_{RO}^S \tau_h} \tag{48}$$

is a material damping term proportional to the ratio between the RO period $T_{RO}^S = 2\pi/\omega_{RO}^S$ and the hole scattering time τ_h.

Compared with Eqs. (29)–(31) corresponding to case S, Eqs. (45)–(47) contain the extra term $-au_h$. From the linearized equations for the zero solution, we obtain the following characteristic equation for $\lambda = \lambda_0$,

$$\lambda_0^3 + a\lambda_0^2 + \lambda_0 + \frac{a}{2} = 0. \tag{49}$$

We analyze the roots of Eq. (49) using a as a parameter. We assume that there is one real root and a pair of complex-conjugate roots.

The expressions for the roots are given in the Appendix. We find that the real root is always negative. The RO frequency is obtained from the imaginary part of the complex conjugate roots. The RO frequency $\omega_{RO}(a)$ given in Eq. (A7) is decreasing from $\omega_{RO} = 1$ $(a \to 0)$ to $\omega_{RO} = 1/\sqrt{2}$ $(a \to \infty)$ (full circles in Fig. 3(a)). The RO damping rate is obtained from the real part of the complex conjugate roots and given in Eq. (A8). The RO damping rate $\Gamma_{RO}(a)$ is first increasing like $\Gamma_{RO} = a/4$ $(a \to 0)$, then reaches a maximum at $a \simeq 1$, and finally decreases like $\Gamma_{RO} = 1/(4a)$ $(a \to \infty)$ (full circles in Fig. 3(b)). For a maximum damping rate, a needs to be close to 1.

In units of the original time t, the RO frequency and damping rate are

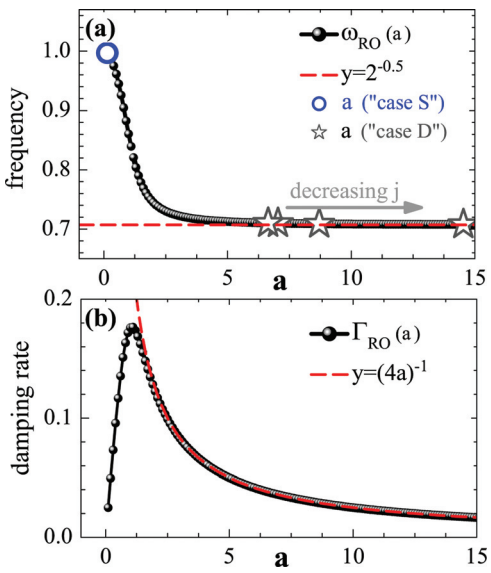

FIG. 3. (Color online) (a) RO frequency and (b) RO damping rate derived in Eqs. (A7) and (A8), respectively, in units of time s as a function of the parameter a introduced in Eq. (48). Gray stars and blue open circles in (a) mark the values of a for different pump currents obtained numerically for case D and case S, respectively, for different pump currents. Dashed red lines indicate analytic approximations for large a.

$$\omega_{RO}^{D} = 2\sqrt{N_{ph}W\kappa}\,\omega_{RO}(a) \tag{50}$$

$$\Gamma_{RO}^{D} = 2\sqrt{N_{ph}W\kappa}\,\Gamma_{RO}(a). \tag{51}$$

We note that these expressions match the results obtained for case S in the limit of small values of a. From the roots of the characteristic equation (49) given in Eqs. (A5) and (A6), we find that $\lambda_{01} = -a/2$ and $\lambda_{02,3} = -a/4 \pm i$ as $a \to 0$. Consequently, $\omega_{RO} \simeq 1$ and $\Gamma_{RO} \simeq a/4$, and the expressions (50) and (51) simplify to

$$\omega_{RO}^{D}(a \to 0) \simeq 2\sqrt{N_{ph}W\kappa}, \tag{52}$$

$$\Gamma_{RO}^{D}(a \to 0) \simeq 1/(4\tau_h). \tag{53}$$

The expression (52) is identical to ω_{RO}^{S} given by Eq. (34). Moreover, we have verified mathematically that the expressions (53) and (42) have a domain of overlap. The limit of small a physically means that the hole capture time τ_h is much larger than the RO period $T_{RO}^{S} = 2\pi/\omega_{RO}^{S}$. The relaxation oscillation properties are then identical to those for quantum well lasers.

If we now consider the case of large a, meaning that the hole capture time is smaller than the RO period, we obtain a different behavior for ω_{RO}^{D} and Γ_{RO}^{D}. From Eqs. (A5) and (A6), we now find that $\lambda_{01} = -a$ and $\lambda_{02,3} = -1/(4a) \pm i/\sqrt{2}$ as $a \to \infty$. Consequently, $\omega_{RO} \simeq 1/\sqrt{2}$ is a constant and $\Gamma_{RO} \simeq 1/(4a)$ displays a hyperbolic law (red dashed lines in Fig. 3(a) and (b)). The expressions (50) and (51) now simplify as

$$\omega_{RO}^{D}(a \to \infty) \simeq \sqrt{2N_{ph}W\kappa}, \tag{54}$$

$$\Gamma_{RO}^{D}(a \to \infty) \simeq \tau_h N_{ph} W\kappa \tag{55}$$

where we have used Eq. (48) for parameter a. The expression for the RO frequency is similar to that in Eq. (34) (except for the factor $\sqrt{2}$). However, the expression of the RO damping rate is clearly dominated by the hole capture time τ_h. In the next section, we concentrate on the large a case and obtain new asymptotic expressions for the RO frequency and RO damping rate. As for the overlap of case S and case D, we will later verify that these new expressions have a domain of overlap with Eqs. (54) and (55).

IV. LARGE SCATTERING RATES FOR HOLES

The RO frequency obtained by Eq. (50) nicely matches the numerically obtained data (black stars and red line in Fig. 2(b)). The gray stars and blue open circles in Fig. 3(a) mark the values of a that we have considered in our numerical simulations of the original laser equations. If we compare the RO damping rate given by Eq. (51) (dash-dotted curve in Fig. 2(c)) with the numerically obtained data (black stars in Fig. 2(c)), a large discrepancy can still be noted. The reason is that the numerically obtained data correspond to relatively large values of a ($6 < a < 15$). In order to improve our asymptotic approximation, we need to consider a as a large parameter and compare it to $\gamma^{-1/2}$.

Our starting point is the analysis of the characteristic Eq. (35) in the limit $\gamma \to 0$. If

$$a = \gamma^{-1/2}\omega a_1 \tag{56}$$

where $a_1 = O(1)$, we note that a distinct asymptotic limit can be obtained. Inserting Eqs. (39) and (56) into Eq. (35) with $\sqrt{\gamma}\omega^{-1}(s_h^{in} + s_h^{out}) = a$, we find from the first two problems for λ_0 and λ_1 that

$$\begin{aligned} \lambda_0 &= \pm i\frac{1}{\sqrt{2}}, \\ \lambda_1 &= -\frac{1}{2a_1}\left[\frac{1}{2} + a_1(s_e^{in} + s_e^{out} + N_{ph} + N_h)\right]. \end{aligned} \tag{57}$$

In units of the original time variable t, the RO frequency and damping rate are given by

$$\omega_{RO}^{Da} = \sqrt{2N_{ph}W\kappa}, \tag{58}$$

$$\begin{aligned} \Gamma_{RO}^{Da} &= \kappa N_{ph} W\tau_h + \frac{1}{2}\tau_e^{-1} + \frac{W}{2}(N_{ph} + N_h) \\ &= \kappa N_{ph} W(\tau_h + (2\kappa)^{-1}) + \frac{1}{2}\tau_e^{-1} + \frac{W}{2}N_h \end{aligned} \tag{59}$$

where the superscript Da means case D with large a. The analytic solutions in Eqs. (58) and (59) have been compared to the numerically obtained values in Fig. 2 and we note their good agreement. We have verified that Eqs. (58) and (59) and Eqs. (54) and (55) have a domain of overlap. To illustrate the magnitude of the different terms contributing to Eq. (59), they are plotted in Fig. 4(a). It can be seen that the photon lifetime $1/(2\kappa)$ and the inverse electron lifetime τ_e^{-1} dominate the damping rate.

Let us now discuss the analytic solutions for the RO frequency and damping rate and derive the K-factor which estimates the maximum intrinsic modulation bandwidth. The K-factor is defined by the relation $\Gamma_{RO}^{Da} = K(\omega_{RO}^{Da})^2/(2\pi)^2$ given in Refs. 22 and 23. We first notice that τ_h and τ_e contribute differently to the damping rate in Eq. (59) (see Fig. 4(a)), and either the hole capture time τ_h or the electron capture time τ_e may play a dominant role in the K-factor depending on the RO frequency. For low values of the RO frequency the contribution of the electron capture is sufficiently larger and the K-factor is nearly completely determined by

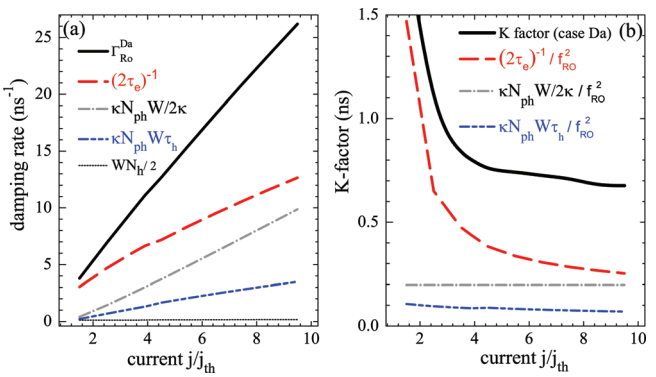

FIG. 4. (Color online) (a) Different contributions to the damping rate as derived in Eq. (59). (b) Total K-factor of the QD laser discussed with case Da (black solid line) and contributions to the K-factor according to Eq. (59) resulting from the electron lifetime (red dashed line), the photon lifetime (gray dash-dotted line), and the hole lifetime (blue dash-dot-dotted line).

$2\pi^2\tau_e^{-1}(\omega_{RO}^{Da})^{-2} = \pi^2(\tau_e N_{ph} W\kappa)^{-1}$, as can be seen in Fig. 4(b), which shows the K-factor (solid line) and the contribution resulting from the electrons (red dashed line). The electron capture time is weakly sensitive to the temperature change,[24] and experimentally reported modulation efficiency and K-factors are nearly constant up to 70°C.[28]

For larger values of the RO frequency (obtained if the laser is pumped with currents far above threshold), the term $2\pi^2\tau_e^{-1}(\omega_{RO}^{Da})^{-2}$ (red dashed line in Fig. 4(b)) becomes small, as can be seen by extrapolating Fig. 4(b) to much higher currents. Thus, in this case, we find that K is given by

$$K = \frac{4\pi^2}{2}(\tau_h + (2\kappa)^{-1}). \tag{60}$$

The K-factor in Eq. (60) linearly depends on the cavity lifetime $(2\kappa)^{-1}$ and the fast hole hole capture time τ_h. The dependence on the cavity lifetime was investigated and fully confirmed experimentally.[25] The holes are thermally distributed and τ_h possesses a temperature dependence based on Fermi statistics. Because the K-factor linearly scales with τ_h, this explains its change with temperature. The linear dependence of the K-factor on the capture time τ_h has previously been attributed to gain compression[23,26] to explain experimental observations of temperature dependent modulation characteristics of a QD laser. Our analysis shows that the K-factor is proportional to τ_h as an intrinsic property of a QD laser without the need of additional assumptions.

V. DISCUSSION

We have determined analytical expressions for the RO frequency and RO damping rate for three different ranges of parameters, which can be classified in terms of the product $\tau_h\omega_{RO}^S$. They are given by case S ($\tau_h\omega_{RO}^S \gg 1$), case D ($\tau_h\omega_{RO}^S = O(1)$), and case Da ($\tau_h\omega_{RO}^S \ll 1$). Our results show that the RO frequency does not explicitly depend on the details of the carrier-carrier scattering between WL and QD. It strongly depends on the cavity lifetime $(2\kappa)^{-1}$ and the radiative recombination lifetime W^{-1}.

The damping rate Γ_{RO}, in contrast, is crucially affected by the carrier-carrier scattering rates. For equal lifetimes of electrons and holes the damping decreases with increasing lifetimes of τ_e and τ_h (see Eq. (42) and recall that $s_e^{in} + s_e^{out}$ and $s_h^{in} + s_h^{out}$ are proportional to τ_e^{-1} and $\tau_h{}^{-1}$, respectively). If both carrier types have different lifetimes, the damping rate increases as the fastest species lifetime increases (in our case D, τ_h; see Eq. (53) or Eq. (59)). Figure 3 is representative of the nonlinear behavior of the RO frequency and damping rate. In particular, the damping rate first increases and then decreases, suggesting that there is an optimal value of parameter a for maximum damping. This result of practical engineering interest could not be anticipated without the help of the analytic analysis.

Our analytical approximations are in very good agreement with numerical simulations of the original laser equations for different doping densities.[9] In Ref. 9, it was shown that increasing n-doping concentration in a case D QD laser leads to a decrease of the electron lifetime, which was at the same time accompanied by increased damping. With the analytical formula given in Eq. (59) the increased damping can be explained by the decreased lifetime (the term with $s_e^{in} + s_e^{out} \sim \tau_e^{-1}$ increases). On the other hand, p-doping of the same device did not yield a higher RO damping. The reason for this counterintuitive result is the separation of timescales of electron and hole lifetimes (which is, for example, the case for materials with large differences in the effective masses of electrons and holes). The slowest species determines the dynamics and, thus, manipulating its lifetime has a drastic effect on the laser dynamics (see Eq. (59)). Instead, manipulating the lifetime of the fast species has only a minor effect. The reduced damping for p-doping concentration is based on a reduction of the electron lifetimes which has its physical origin in the increased rate for mixed electron-hole Coulomb scattering processes due to the excess holes in the reservoir. It confirms that p-doping is beneficial for the modulation response of QD lasers.[27] If a high RO damping rate is a desired property of QD lasers, n-doping should be helpful.

ACKNOWLEDGMENTS

The work of K. Lüdge and E. Schöll was supported by DFG in the framework of Sfb 787. The work by E. Viktorov and T. Erneux was supported by the Fond National de la Recherche Scientifique (Belgium). The research by T. Erneux was also supported by the Air Force Office of Scientific Research (AFOSR) grant FA8655-09-1-3068.

APPENDIX: ROOTS OF THE CHARACTERISTIC EQUATION

We determine the roots of Eq. (49). From Abramowitz and Stegun,[29] we first determine q and r as

$$\begin{aligned} q &= \frac{1}{3} - \frac{a^2}{9}, \\ r &= \frac{1}{6}(a - \frac{3}{2}a) - \frac{a^3}{27} = -\frac{a}{12} - \frac{a^3}{27}. \end{aligned} \tag{A1}$$

Assuming $q^3 + r^2 > 0$, we have one real root and a pair of complex conjugate roots. From

$$\begin{aligned} s_1 &\equiv \left[r + \sqrt{q^3 + r^2}\right]^{1/3}, \\ s_2 &\equiv \left[r - \sqrt{q^3 + r^2}\right]^{1/3}, \end{aligned} \tag{A2}$$

we obtain

$$s_1 = \left[-\frac{a}{12} - \frac{a^3}{27} + \frac{1}{9}\sqrt{3 - 3 \times \frac{117}{144}a^2 + \frac{3}{2}a^4}\right]^{1/3}, \tag{A3}$$

$$s_2 = \left[-\frac{a}{12} - \frac{a^3}{27} - \frac{1}{9}\sqrt{3 - 3 \times \frac{117}{144}a^2 + \frac{3}{2}a^4}\right]^{1/3}. \tag{A4}$$

The three roots are then given by

$$\lambda_{01} = s_1 + s_2 - \frac{a}{3} \tag{A5}$$

$$\lambda_{02,3} = -\frac{1}{2}(s_1 + s_2) - \frac{a}{3} \pm \frac{i\sqrt{3}}{2}(s_1 - s_2). \tag{A6}$$

The expression for the RO frequency is the imaginary part of Eq. (A6). The expression for the RO damping rate is provided by the absolute value of the real part of Eq. (A6). They are given by

$$\omega_{RO}(a) = \frac{i\sqrt{3}}{2}(s_1 - s_2) \tag{A7}$$

$$\Gamma_{RO}(a) = \frac{1}{2}(s_1 + s_2) + \frac{a}{3}. \tag{A8}$$

[1]D. Bimberg, M. Grundmann, and N. N. Ledentsov, *Quantum Dot Heterostructures* (John Wiley & Sons, New York, 1999).
[2]M. Kuntz, N. N. Ledentsov, D. Bimberg, A. R. Kovsh, V. M. Ustinov, A. E. Zhukov, and Y. M. Shernyakov, Appl. Phys. Lett. **81**, 3846 (2002).
[3]M. Sargent, M. O. Scully, and W. E. Lamb, *Laser Physics* (Addison-Wesley, Reading, MA, 1974).
[4]H. Haken, *Licht und Materie 2* (Bibliographisches Institut, Mannheim, Germany, 1981).
[5]K. Petermann, *Laser Diode Modulation and Noise* (KTK Scientific, Tokyo, 1988).
[6]G. P. Agrawal and N. K. Dutta, *Semiconductor Lasers* (Van Nostrand Reinhold, New York, 1993).
[7]H. Risken and K. Nummedal, J. Appl. Phys. **39**, 4662 (1968).
[8]K. Lüdge and E. Schöll, IEEE J. Quantum Electron. **45**, 1396 (2009).
[9]K. Lüdge and E. Schöll, Eur. Phys. J. D **58**, 167 (2010).
[10]N. Majer, K. Lüdge, and E. Schöll, Phys. Rev. B **82**, 235301 (2010).
[11]M. Wegert, N. Majer, K. Lüdge, S. Dommers-Völkel, J. Gomis-Bresco, A. Knorr, U. Woggon, and E. Schöll, Semicond. Sci. Technol. **26**, 014008 (2011).
[12]E. A. Viktorov, T. Erneux, P. Mandel, T. Piwonski, G. Madden, J. Pulka, G. Huyet, and J. Houlihan, Appl. Phys. Lett. **94**, 263502 (2009).
[13]T. Piwonski, J. Pulka, G. Madden, G. Huyet, J. Houlihan, E. A. Viktorov, T. Erneux, and P. Mandel, Appl. Phys. Lett. **94**, 123504 (2009).
[14]T. Erneux, E. A. Viktorov, P. Mandel, T. Piwonski, G. Huyet, and J. Houlihan, Appl. Phys. Lett. **94**, 113501 (2009).
[15]D. Goulding, S. P. Hegarty, O. Rasskazov, S. Melnik, M. Hartnett, G. Greene, J. G. McInerney, D. Rachinskii, and G. Huyet, Phys. Rev. Lett. **98**, 153903 (2007).
[16]T. Erneux, E. A. Viktorov, B. Kelleher, D. Goulding, S. P. Hegarty, and G. Huyet, Opt. Lett. **35**, 070937 (2010).
[17]D. O'Brien, S. P. Hegarty, G. Huyet, and A. V. Uskov, Opt. Lett. **29**, 1072 (2004).
[18]G. Huyet, D. O'Brien, S. P. Hegarty, J. G. McInerney, A. V. Uskov, D. Bimberg, C. Ribbat, V. M. Ustinov, A. E. Zhukov, S. S. Mikhrin, A. R. Kovsh, J. K. White, K. Hinzer, and A. J. SpringThorpe, Phys. Status Solidi B **201**, 345 (2004).
[19]C. Otto, K. Lüdge, and E. Schöll, Phys. Status Solidi B **247**, 829 (2010).
[20]E. Malić, K. J. Ahn, M. J. P. Bormann, P. Hövel, E. Schöll, A. Knorr, M. Kuntz, and D. Bimberg, Appl. Phys. Lett. **89**, 101107 (2006).
[21]T. Erneux and P. Glorieux, *Laser Dynamics* (Cambridge University Press, Cambridge, UK, 2010).
[22]R. Olshansky, P. Hill, V. Lanzisera, and W. Powazinik, IEEE J. Quantum Electron. **23**, 1410 (1987).
[23]D. Klotzkin and P. Bhattacharya, J. Lightwave Technol. **17**, 1634 (1999).
[24]K. Lüdge, R. Aust, G. Fiol, M. Stubenrauch, D. Arsenijević, D. Bimberg, and E. Schöll, IEEE J. Quantum Electron. **46**, 1755 (2010).
[25]M. Ishida, N. Hatori, T. Akiyama, K. Otsubo, Y. Nakata, H. Ebe, M. Sugawara, and Y. Arakawa, Appl. Phys. Lett. **85**, 4145 (2004).
[26]A. Fiore and A. Markus, IEEE J. Quantum Electron. **43**, 287 (2007).
[27]O. B. Shchekin and D. G. Deppe, Appl. Phys. Lett. **80**, 2758 (2002).
[28]Y. Arakawa and M. Sugawara, Proc. SPIE **5722**, 45 (2005).
[29]M. Abramowitz and I.A. Stegun, *Handbook of Mathematical Functions* (Dover, New York, 1964)